Intermodal Four-Wave-Mixing and Parametric Amplification in km-long Multi-Mode Fibers

Massimiliano Guasoni, Francesca Parmigiani, Peter Horak, Julien Fatome, and David J. Richardson

***Abstract*—We theoretically and numerically investigate intermodal four-wave-mixing in km-long fibers, where random birefringence fluctuations are present along the fiber length. We identify several distinct regimes that depend on the relative magnitude between the length scale of the random fluctuations and the beat lengths of the interacting quasi-degenerate modes. In addition, we analyze the impact of mode dispersion and we demonstrate that random variations of the core radius, which are typically encountered during the drawing stage of the fiber, can represent the major source of bandwidth impairment. These results set a boundary on the limits of validity of the classical Manakov model and may be useful for the design of multimode parametric amplifiers and wavelength converters, as well as for the analysis of nonlinear impairments in long-haul spatial division multiplexed transmission.**

***Index Terms*—Four-wave mixing (FWM), nonlinear optics, optical amplifiers, optical wavelength conversion.**

I. Introduction

In the last decade there has been intense research in space-division multiplexing (SDM) schemes [1] and novel all-optical devices for signal processing [2]. Both these hot topics aim to develop new generation high-capacity internet networks capable of responding to the exponential growth of data demand. Within this framework, intermodal four-wave mixing (IM-FWM) in km-long multi-mode fibers (MMFs) is a key nonlinear process to be investigated for two main reasons. First, FWM is one of the main impairments affecting SDM transmissions [3]. Second, the use of long fibers leads to large degrees of nonlinearity even at low input powers. This increases the overall efficiency of FWM-based devices and paves the way for the development of all-optical devices that may overcome the main limits associated with single-mode fiber-based devices. Specifically, the phase-matching condition in IM-FWM processes can be achieved far away from both the zero dispersion wavelength and the bandwidth of spontaneous Raman scattering, thus reducing the impact of the nonlinear cross-talk and of the Raman noise contribution [4].

When analyzing light propagation in km-long fibers, it is important to take into account random birefringence fluctuations that occur on a length scale ranging from a few meters to several tens of meters [5], [6]. These fluctuations are caused by manufacturing imperfections, environmental variations or local stress mechanisms and impair the FWM dynamics by inducing linear coupling among quasi-degenerate modes. Recently, the experimental demonstration of IM-FWM in km-long fibers has been reported [4], [7]. Moreover, while intramodal FWM in km-long single-mode fibers has been theoretically analyzed for a long time [8], [9], [10], theoretical studies related to intermodal FWM in MMFs are quite recent [11], [12], [13], [14], [15], [16], [17], [18].

Differently from past works, here we study the IM-FWM dynamics as function of the degree of randomicity in the fiber. We introduce some characteristic lengths that define the main fiber features in the presence of random perturbations and we distinguish two different kinds of perturbations.

The first is related to random fluctuations of the birefringence axes, which lead to a linear coupling between the quasi-degenerate modes of the fiber. Depending on the relative magnitude among the aforementioned characteristic lengths, we distinguish different FWM regimes: the fiber may exhibit an "isotropic"-like behavior or a fully random coupling dynamics between quasi-degenerate modes which is described by the Generalized Manakov Model for MMFs [19], [20], [21]. These results set a boundary on the limits of validity of the classical Manakov model and therefore provide new perspectives for multimode long-haul transmission, similarly to what has recently been observed in single-mode fibers [22].

The second kind of perturbation is related to random variations of the dispersion parameters of the different modal groups. We demonstrate that these variations, along with mode dispersion, represent the main source of IM-FWM impairment. These novel outcomes could give useful guidelines for both the mitigation of FWM in SDM transmission and for the design of all-optical devices for signal processing.

The paper is organized as follows. In Section II we introduce the characteristic lengths . In Section III we model the random birefringence fluctuations and the induced linear coupling among quasi-degenerate modes of a MMF. In Section IV we discuss the existence of the different FWM regimes related to the aforementioned characteristic lengths. In Section V the impact of mode dispersion on IM-FWM is analysed. Finally, in Section VI we address the influence of random fluctuations of the dispersion parameters.

Manuscript received XXX.

M. Guasoni is supported through an Individual Marie Sklodowska- Curie Fellowship (H2020 MSCA IF 2015 , project AMUSIC - Grant Agreement 702702). This research is sponsored by EPSRC grant EP/P026575/1.

M. Guasoni, F. Parmigiani, P. Horak, and D. J. Richardson are with the Optoelectronics Reserch Centre, University of Southampton, Southampton SO17 1BJ, United Kingdom.

J. Fatome is with the Laboratoire Interdisciplinaire Carnot de Bourgogne (ICB), UMR 6303 CNRS - Université Bourgogne Franche-Comté, 9 Avenue Alain Savary, BP 47870, 21078 Dijon, France

M. Guasoni's email is m.guasoni@soton.ac.uk

II. Modeling of random birefringence fluctuations

In the weakly guiding approximation, circular core isotropic fibers are characterized by groups of modes that are two-fold (groups LP_{0k}) or four-fold (groups LP_{hk}, with $h \geq 1$ integer) degenerate. Degenerate modes of the same group possess identical dispersion parameters. However, in real optical fibers various random imperfections break the circular symmetry and isotropy of the fiber. Each degenerate mode is affected in a different way by these perturbations: as a result degenerate modes of the same group separate into a set of distinct quasi-degenerate modes, each one characterized by its own dispersive properties.

The exact modeling of each source of perturbation is cumbersome and is still an active topic of research [23], [24], [25]. On the other hand, their global effect is that of a local and asymmetric weak variation of the fiber cross-section shape and size, as well as of the refractive index, giving rise to a weak local birefringence whose axes move randomly along the fiber [26]. We take as a reference the fast axis of the fiber and indicate with $\alpha(z)$ its angular orientation at the position z along the fiber. As the perturbations are typically weak, we can safely assume that the shape of the modes is preserved. What changes instead is the orientation of their electric field, which is aligned to the local axes of birefringence and is thus either parallel or orthogonal to $\alpha(z)$ (see Fig. 1). Furthermore, each mode has its own propagation constant $\beta(z)$, inverse group velocity $\beta_1(z) = \partial\beta/\partial\omega$ and chromatic dispersion $\beta_2(z) = \partial^2\beta/\partial\omega^2$ that are generally $z-$dependent.

In the following, for the sake of simplicity, we neglect higher-order dispersion and we assume the two groups of modes involved in the IM-FWM process are the LP_{01} and the LP_{11}. Note however that the main outcomes in this paper can be easily generalized to include the interaction between different groups of modes and the presence of higher-order dispersion terms. We denote by $0p$ and $0o$ the two quasi-degenerate modes of group LP_{01} that are polarized respectively parallel (p) or orthogonal (o) to α. Similarly, we denote by $1ap$, $1bp$, $1ao$ and $1bo$ the four quasi-degenerate modes of the group LP_{11}, as illustrated in Fig. 1.

The angle $\alpha(z)$ changes randomly along the fiber length and is characterized by a correlation length, L_C, which defines the length-scale over which random perturbations become uncorrelated. As previously outlined, in typical standard fibers, L_C varies from a few meters to some tens of meters.

For each pair of quasi-degenerate modes, e.g. $mode1$ and $mode2$, we can define a corresponding beat length $L_{B(mode1-mode2)} = 2\pi/(\beta_{mode1} - \beta_{mode2})$. In the problem under analysis there are 4 independent beat lengths, $L_{B(0p-0o)}$, $L_{B(1ap-1ao)}$, $L_{B(1ap-1bp)}$ and $L_{B(1ap-1bo)}$, from which the 3 remaining beat lengths can be computed (e.g., $L^{-1}_{B(1bp-1ao)} = L^{-1}_{B(1ap-1ao)} - L^{-1}_{B(1ap-1bp)}$). While beat lengths are generally z-dependent, the FWM dynamics is mainly sensitive to their spatial average (see Section IV). Therefore, in what follows we refer to their spatial average. The beat length is indicative of the length scale over which the two quasi-degenerate modes acquire a significant phase

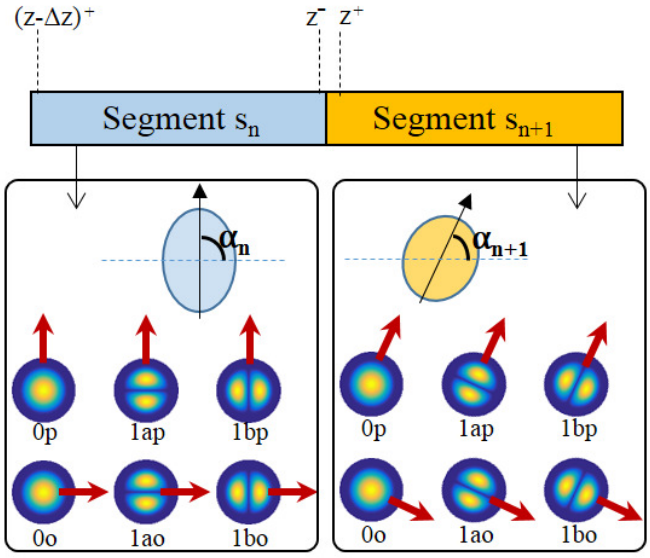

Fig. 1. Schematic of multimode randomly birefringent fiber. Two consecutive segments of fiber, s_n ans s_{n+1}, are displayed. Each segment has its own cross-section shape (elliptic in this figure) characterized by a particular angle, α_n and α_{n+1} respectively, defining the direction of the fast birefringence axis (black solid arrow). Modes of groups LP_{01} and LP_{11} are shown for the two segments. Both the electric field (solid red arrow) and the axis of symmetry of each mode are aligned parallel or orthogonal to the fast birefringence axis. Points z^- and z^+ are also shown, representing respectively the positions immediately before and after the entry in segment s_{n+1}. Similarly, point $(z-\Delta z)^+$ is the position immediately after the entry in segment s_n.

difference and thus of the minimum fiber length L which is necessary to distinguish them. Typically, the stronger the local perturbations, the larger is the difference between the two propagation constants, thus the shorter the corresponding beat length. Therefore, the correlation length L_C is a measure of "how fast" random perturbations occur, whereas the beat lengths among quasi-degenerate modes measure "how strong" these perturbations are. If the fiber length L is much shorter than all the beat lengths, that is $L \ll \min\{|L_B|\}$, then modes within the same group propagate together in phase. In other words: in this instance random perturbations are weak enough so that the fiber can be considered perfectly circular and isotropic along its whole length. It is worth noting that beat lengths can vary across a range of values from a few meters to tens of meters. For this reason, typical isotropic fibers are a few tens of meters long, so that relevant degrees of nonlinearity can only be achieved at the expenses of a large amount of input power. In the following, however, we are interested in km-long fibers, for which even small power levels may give rise to significant nonlinear effects. Therefore, in the following we can safely assume $L \gg \max\{|L_B|\}$, where $\max\{|L_B|\}$ is the largest beat length.

The relative magnitude between the characteristic lengths discussed here gives rise to different FWM regimes that will be analyzed in the next sections.

III. Random coupling induced by perturbations

To understand the coupling mechanism induced by random perturbations, it is useful to represent the fiber as a

concatenation of short segments of length Δz (see Fig. 1). Each segment is short enough to preserve, along its whole length, both the direction α of the birefringence axes and the dispersion parameters of all modes. Let us consider light propagation in two consecutive segments s_n and s_{n+1}. Segment s_n (s_{n+1}) is characterized by its own direction α_n (α_{n+1}), with respect to which the electric field of the modes is parallel or orthogonal. We indicate with $\mathbf{A}(z) = [A_{0p}(z), A_{0o}(z), A_{1ap}(z), A_{1ao}(z), A_{1bp}(z), A_{1bo}(z)]$ the vector of the corresponding 6 modal amplitudes. Note that here and throughout the whole paper variables written in bold font indicate a vector or a matrix. Modes of segment s_n, immediately before entering s_{n+1}, are projected onto the modes of s_{n+1} (see Appendix I for details). The projection is described by the following linear relation: $\mathbf{A_{n+1}^{(in)}} = \mathbf{P}\mathbf{A_n^{(out)}}$, where $\mathbf{A_n^{(out)}} \equiv \mathbf{A}(z^-)$ is the vector of amplitudes at point z^-, at the end of s_n and just before entering s_{n+1}, and $\mathbf{A_{n+1}^{(in)}} \equiv \mathbf{A}(z^+)$ is the vector at point z^+, just after entering s_{n+1} (Fig. 1). The projection matrix reads:

$$\mathbf{P} = \begin{bmatrix} C & -S & 0 & 0 & 0 & 0 \\ S & C & 0 & 0 & 0 & 0 \\ 0 & 0 & C^2 & -SC & -SC & S^2 \\ 0 & 0 & SC & C^2 & -S^2 & -SC \\ 0 & 0 & SC & -S^2 & C^2 & -SC \\ 0 & 0 & S^2 & SC & SC & C^2 \end{bmatrix} \quad (1)$$

where $C = \cos(\Delta\alpha)$ and $S = \sin(\Delta\alpha)$, with $\Delta\alpha = \alpha_{n+1} - \alpha_n$. According to this model, coupling among different quasi-degenerate modes is thus induced by the random variation $\Delta\alpha$ of the birefringence axes. If no variation occurs, i.e. $\Delta\alpha = 0$, then there is no energy exchange within quasi-degenerate modes ($\mathbf{A_{n+1}^{(in)}} = \mathbf{A_n^{(out)}}$), which is consistent with the assumption that the modal shape is largely preserved along the fiber length. Note also that according to matrix $\mathbf{P}$ there is no linear coupling between a mode of group LP_{01} and a mode of group LP_{11}. In practice, such coupling exists as a result of a different kind of perturbations [23], [24], but FWM-induced coupling is typically negligible because of the large difference in the propagation constants between the two mode groups [11], [14].

In order to describe the propagation in the fiber, we study the evolution of light from point $(z-\Delta z)^+$, at the entry of segment s_n, to the point z^+, at the entry of s_{n+1}. First, light propagates through the segment s_n from $(z-\Delta z)^+$ to z^-, undergoing both dispersion (operator $\hat{D}$) and nonlinearity (operator $\hat{N}$): $\mathbf{A_n^{(out)}} - \mathbf{A_n^{(in)}} = \Delta z[\hat{D}\{\mathbf{A_n^{(in)}}\} + \hat{N}\{\mathbf{A_n^{(in)}}\}]$, where $\mathbf{A_n^{(out)}} - \mathbf{A_n^{(in)}}$ indicates the mode amplitude variation, with $\mathbf{A_n^{(in)}} \equiv \mathbf{A}((z-\Delta z)^+)$. Then, modes of segment s_n are projected onto modes of s_{n+1} according to the relation $\mathbf{A_{n+1}^{(in)}} = \mathbf{P}\mathbf{A_n^{(out)}}$. From the two aforementioned relations, we finally evaluate the derivative $\partial\mathbf{A}/\partial z = \lim_{\Delta z \to 0}(\mathbf{A_{n+1}^{(in)}} - \mathbf{A_n^{(in)}})/\Delta z$, which after some algebra takes the form of the following Nonlinear Schrödinger Equation (NLSE):

$$\begin{aligned} \partial_z \mathbf{A} = \quad & \bar{\mathbf{Q}}\mathbf{A} - \mathbf{t}\mathbf{A} - (\bar{\boldsymbol{\beta}}_\mathbf{1} - v_r^{-1})\partial_t \mathbf{A} - i(1/2)\bar{\boldsymbol{\beta}}_\mathbf{2}\partial_{tt}\mathbf{A} + \\ & + \hat{N}\{\mathbf{A}\} + i\tilde{\boldsymbol{\beta}}\mathbf{A} - \tilde{\boldsymbol{\beta}}_\mathbf{1}\partial_t\mathbf{A} - i(1/2)\tilde{\boldsymbol{\beta}}_\mathbf{2}\partial_{tt}\mathbf{A} \quad (2) \end{aligned}$$

In Eq. (2) each dispersion coefficient is separated into the sum of its spatial average (accent $\bar{}$) and its $z-$varying part (accent $\tilde{}$) . This separation is introduced because, as will be discussed in Section VI, the averages and varying parts play a different role in the IM-FWM dynamics.

The 6x6 matrix $\bar{\mathbf{Q}} = i\bar{\beta} + \partial_z\alpha\mathbf{U}$, where the matrix $\mathbf{U}$ is reported in Appendix I. The diagonal matrix $\bar{\boldsymbol{\beta}} = diag[\bar{\beta}_{0p} - R_0, \bar{\beta}_{0o} - R_0, \bar{\beta}_{1ap} - R_1, \bar{\beta}_{1ao} - R_1, \bar{\beta}_{1bp} - R_1, \bar{\beta}_{1bo} - R_1]$ includes the propagation constants and two constant terms R_0 and R_1 corresponding to overall phase factors that can be conveniently chosen as $R_0 = \bar{\beta}_{0p}$ and $R_1 = \bar{\beta}_{1ap}$. Note that R_0 and R_1 can be chosen independently of each other only under the assumption that there is a large difference between the propagation constants of modes in group LP_{01} and modes in group LP_{11}. The matrix $\mathbf{t} = diag[t_{0p}, t_{0o}, t_{1ap}, t_{1ao}, t_{1bp}, t_{1bo}]$ includes the absorption losses of modes, that for the sake of simplicity are assumed to be constant along the fiber.

Finally, from the definition of the beat lengths in the previous section, one can rewrite the matrix $\bar{\mathbf{Q}} = -i2\pi\bar{\mathbf{L}}_\mathbf{B}^{-1} + \partial_z\alpha\mathbf{U}$, where $\bar{\mathbf{L}}_\mathbf{B} = diag[0, \bar{L}_{B(0p-0o)}, 0, \bar{L}_{B(1ap-1ao)}, \bar{L}_{B(1ap-1bp)}, \bar{L}_{B(1ap-1bo)}]$. Matrix $\bar{\boldsymbol{\beta}}_\mathbf{1} = diag[\bar{\beta}_{1,0p}, \bar{\beta}_{1,0o}, \bar{\beta}_{1,1ap}, \bar{\beta}_{1,1ao}, \bar{\beta}_{1,1bp}, \bar{\beta}_{1,1bo}]$ includes the average inverse group velocity coefficients, whereas v_r is a free parameter that represents the velocity of a reference frame and can be conveniently chosen as $v_r = 1/\bar{\beta}_{1,0p}$. Matrix $\bar{\boldsymbol{\beta}}_\mathbf{2} = diag[\bar{\beta}_{2,0p}, \bar{\beta}_{2,0o}, \bar{\beta}_{2,1ap}, \bar{\beta}_{2,1ao}, \bar{\beta}_{2,1bp}, \bar{\beta}_{2,1bo}]$ includes the average chromatic dispersion coefficients. The matrices $\tilde{\boldsymbol{\beta}}_\mathbf{1}$ and $\tilde{\boldsymbol{\beta}}_\mathbf{2}$ are formed analogously to $\bar{\boldsymbol{\beta}}_\mathbf{1}$ and $\bar{\boldsymbol{\beta}}_\mathbf{2}$ by replacing the average parameter $\bar{x}$ with the z-varying part $\tilde{x}$. Finally, matrix $\tilde{\boldsymbol{\beta}} = diag[\tilde{\beta}_{0p}, \tilde{\beta}_{0o}, \tilde{\beta}_{1ap}, \tilde{\beta}_{1ao}, \tilde{\beta}_{1bp}, \tilde{\beta}_{1bo}]$. The operator $\hat{N}$ accounts for all nonlinear multimode interactions, as discussed in [27]. **However, in order to focus on the role of FWM in the nonlinear dynamics, in our simulations we only consider Kerr nonlinearity and ignore the Raman contribution.** In the following we assume that the chromatic dispersion of modes within the same group is the same, indicating with $\beta_{2,0}$ the coefficients $\beta_{2,0p} = \beta_{2,0o}$ and with $\beta_{2,1}$ the coefficients $\beta_{2,1ap} = \beta_{2,1a0} = \beta_{2,1bp} = \beta_{2,1bo}$. We point out that all the dispersion coefficients and the beat-lengths of Eq. (2) are computed at a common reference frequency.

It is worth noting that Eq. (2) represents a generalization of the approach introduced in [26] to describe the effects of birefringence fluctuations in single-mode fibers. Note also that vector $\mathbf{A}$ in Eq. (2) describes the modal amplitudes in the local reference frame, which is defined by the orientation $\alpha(z)$.

Similarly to previous work [11], in Eq. (2) the overall effect of linear coupling is described by a 6x6 matrix $\bar{\mathbf{Q}}$. However, a major advantage of our approach is that this matrix is explicitly written in terms of the main real fiber parameters, that are the average beat lengths among quasi-degenerate modes and the function $\alpha(z)$ which accounts for the random evolution of the birefringence axes. We can therefore study light propagation versus different profiles of $\alpha(z)$ and of beat lengths, and identify different regimes that are discussed in the next Section.

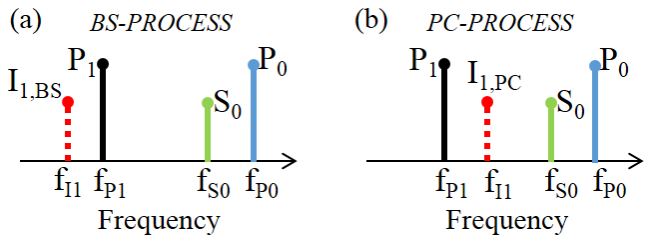

Fig. 2. (a) Representation of Bragg scattering. The input waves P_0, P_1 and S_0 generate the idler component $I_{1,BS}$. Energy conservation implies $f_{I1} - f_{P1} = f_{S0} - f_{P0}$. (b) Representation of phase conjugation. Energy conservation implies $f_{I1} - f_{P1} = f_{P0} - f_{S0}$.

IV. From Uncoupled to the Manakov Regime

In this Section we study the impact of random perturbations on two important IM-FWM processes, namely Bragg scattering (BS) and phase conjugation (PC) [28]. The configuration of the corresponding processes is represented in Fig. 2, where two input pumps P_0 and P_1 are coupled to modes LP_{01} and LP_{11}, respectively, and an input seed signal S_0 is coupled to mode LP_{01}. Due to IM-FWM new idlers in the corresponding LP_{11} mode group are generated for both the BS ($I_{1,BS}$) and the PC processes ($I_{1,PC}$). All the waves are monochromatic and we indicate with f_{P0}, f_{S0}, f_{P1} and f_{I1} their corresponding frequency. Note that the pump frequency f_{P0} plays the role of a reference frequency in Eq. (2), that is, all the dispersion coefficients and the beat lengths are computed at f_{P0}. We analyze the idler growth as a function of the system parameters, computing the idler power as the sum of the powers in the 4 quasi-degenerate LP_{11} modes.

We initially assume that the dispersion coefficients are constant along the fiber length (that is, $\tilde{\boldsymbol{\beta}} = \tilde{\boldsymbol{\beta}}_{\mathbf{1}} = \tilde{\boldsymbol{\beta}}_{\mathbf{2}} = 0$ in Eq. (2)); the effects of their $z-$dependence will be discussed later. We also assume the pumps and signal are linearly copolarized, which maximizes the idler growth. For the fiber parameters used here we refer to the graded-index fiber employed in [29] . We fix $v_{0p} - v_{1ap} = 100$ ps/km, whereas the chromatic dispersion coefficients are fixed respectively to 19.8 ps/(nm km) for both modes of group LP_{01} and to 21.8 ps/(nm km) for all modes of group LP_{11}. **The effective areas for modes of groups LP_{01} and LP_{11} are $161\mu m^2$ and $170\mu m^2$, respectively. Since the modes of graded-index fibers can be approximated as Hermite-Gaussian functions [30], from the knowledge of the effective areas we can estimate their transverse profile. Finally, the nonlinear overlap coefficients are computed as reported in Ref.[27]. Here they are indicated as** C_{abcd}. Indices $\{a, b, c, d\}$ are employed to refer to the modes: the index 0 refers to one of the modes $0p$ and $0o$; 1 refers to one of the modes $1ap$ and $1ao$; 2 refers to one of the modes $1bp$ and $1bo$. Due to the symmetries of the modes under consideration, the coefficients with subscripts of the kind $aabb$ or $aaaa$ are the only non-zero ones and are invariant with respect to permutations of the indices (e.g. $C_{aabb} = C_{abab}$) [4], [27]. **For the fiber of Ref.[29] we find**: $C_{0000} = 0.63$ km^{-1}W^{-1}; $C_{0011} = C_{0022} = 0.39$ km^{-1}W^{-1}; $C_{1111} = C_{2222} = 0.60$ km^{-1}W^{-1}; $C_{1122} = 0.18$ km^{-1}W^{-1}. Absorption losses are assumed to be 0.2 dB/km and 0.3 dB/km for modes of groups LP_{01} and LP_{11}, respectively. Input powers are 22.5 dBm for each pump and 3.5 dBm for the signal.

In order to get some realistic value for the strength of the random perturbations, we assume the average residual birefringence (that is the difference between the refractive indices of the birefringence axes) to be $\Delta n = 1.5 \cdot 10^{-7}$, which is a typical value for standard optical fibers used in telecommunications. This provides an estimate for the beat length $L_{B(0p-0o)} = \lambda/\Delta n = 10$ m and the inverse group velocity mismatch $\beta_{1,0p} - \beta_{1,0o} = \Delta n/c = 0.5$ ps/km, where $\lambda = 1550$ nm is the wavelength of the pump in mode $0p$. We use values of the same order for the beat lengths and inverse group velocity mismatches of the group LP_{11}: $L_{B(1ap-1ao)} = 25$ m; $L_{B(1ap-1bp)} = 50$ m; $L_{B(1ap-1bo)} = 8$ m; $\beta_{1,ap} - \beta_{1,1ao} = 0.2$ ps/km; $\beta_{1,ap} - \beta_{1,1bp} = 0.4$ ps/km; $\beta_{1,1ap} - \beta_{1,1bo} = 0.6$ ps/km.

The phase matching condition of IM-FWM processes in an isotropic fiber is fulfilled when the sum of the inverse group velocities of the pump and signal in group LP_{01} equates to the sum of the inverse group velocities of the pump and signal in group LP_{11} [4], [11], which is derived by a Taylor expansion of the propagation constants for the two mode groups. Therefore, phase matching is essentially related to the dispersion properties of the different mode groups. In randomly perturbed fibers, the small differences of group velocity among quasi-degenerate modes do not significantly affect the IM-FWM phase matching. Therefore the aforementioned phase-matching condition can be safely rewritten as $\beta_{1,0p}(f_{P0}) + \beta_{1,0p}(f_{S0}) = \beta_{1,ap}(f_{P1}) + \beta_{1,ap}(f_{I1})$.

We first study the BS process (Fig. 2a). We simulate Eq. (2) using the system parameters illustrated above and with a pump-to-pump detuning $f_{P0} - f_{P1} = 0.575$ THz, which corresponds to the phase-matching condition for the BS process. The signal-to-pump detuning $f_{S0} - f_{P0}$ spans from -0.5 THz to -0.1 THz. Moreover, we generate random smooth profiles for $\alpha(z)$ with vanishing spatial average and different values of correlation length L_C. In our simulations L_C is defined on the basis of the correlation function $C_\alpha(z) = |\int \alpha(z')\alpha(z'-z)dz'|/\int \alpha(z')^2 dz'$; it indicates the length beyond which the correlation function remains below 0.1, that is $C_\alpha(z > L_C) < 0.1$. Simulation results are displayed in Fig. 3 and show the existence of 3 distinct regimes depending on the relative magnitude between L_C and the beat lengths. For values of $L_C > 5 \cdot \max\{|L_B|\}$, as in the case of $L_C = 260$ m in Fig. 3, the idler dynamics does not depend on the particular value of L_C and resembles the dynamics found for $L_C = \infty$, i.e. when the angle $\alpha(z)$ does not vary along the fiber length. In this instance, here named the *Uncoupled Regime*, random perturbations evolve slowly enough to prevent any significant linear coupling among quasi-degenerate modes. Therefore, the fiber can be considered as a birefringent fiber with fixed axes of birefringence. As such, the idler growth strictly depends on the polarization direction of the copolarized input waves and is maximized when they are aligned to one of the birefringence axes.

In the other extreme, when random fluctuations are fast

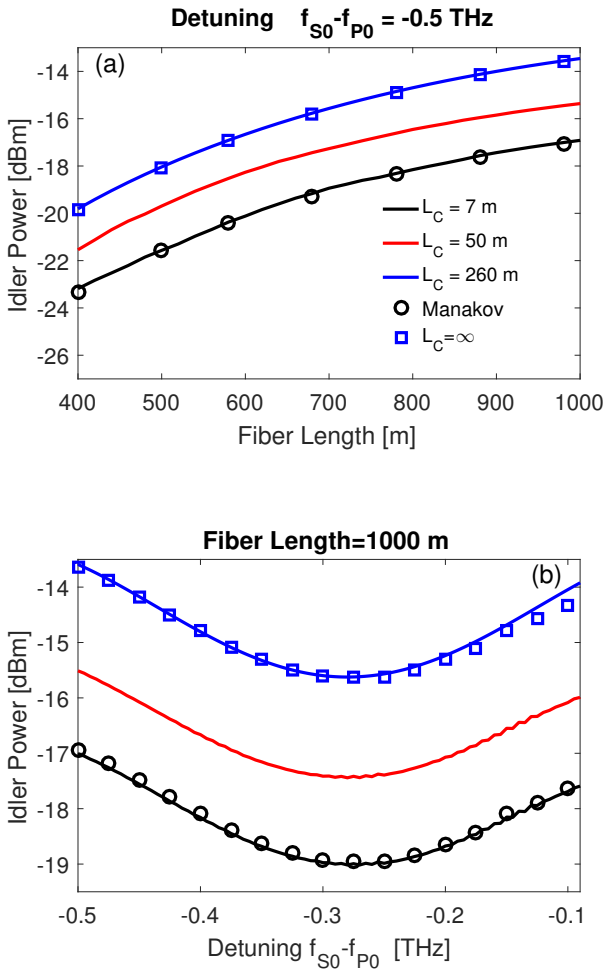

Fig. 3. BS process. (a) Idler power versus fiber length L for a fixed signal-to-pump detuning $f_{S0} - f_{P0} = -0.5$ THz and for different values of coherence length L_C. The pump-to-pump detuning is $f_{P0} - f_{P1} = 0.575$ THz, which maximizes the phase-matching. The case $L_C = \infty$ (fixed axes of birefringence) and the solution of the multimode Manakov model are also reported. (b) Idler power versus signal-to-pump detuning for a fixed fiber length $L = 1000$ m.

and take place on a length scale shorter than the beat lengths ($L_C < \min\{|L_B|\}$, as in the case of $L_C = 7$ m in Fig. 3), the idler growth computed by Eq. (2) turns out to be in excellent agreement with the growth obtained by the solution of the multimode Manakov equations [14], [19], [20], [21]. Therefore we refer to this instance as the *Manakov Regime* where, differently from the Uncoupled Regime, the system dynamics is independent of the polarization direction of the copolarized input beams. Following considerations similar to those discussed in [11] we analytically estimate an idler amplification impairment of about -3.5 dB between the Uncoupled Regime and the Manakov Regime, which is confirmed by our numerical results displayed in Fig. 3. Note that this impairment is almost independent of the signal frequency and the fiber length L. However, it is important to notice that this estimate applies only when, in the Uncoupled Regime, the input beams are aligned with one of the axes of birefringence, so that idler growth is maximized.

For intermediate values $\min\{|L_B|\} < L_C < 5\max\{|L_B|\}$ ($L_C = 50$ m in Fig. 3) we find an *Intermediate Regime* where the idler amplification depends on the specific value of L_C.

Differently from the BS process, where phase matching is essentially governed by the pump-to-pump detuning, in the PC process (Fig. 2b) it is mainly related to the signal wavelength [4]. When both pumps are centered at the same frequency (degenerate FWM, $f_{P0} = f_{P1}$) we find that phase matching is optimized for $f_{S0} - f_{P0} = 0.605$ THz. Simulation results are displayed in Fig. 4 when large pump powers (35 dBm) are employed to get efficient idler amplification; the input signal power is -9 dBm. These results demonstrate once again the existence of the 3 distinct regimes observed in the BS process; on the other hand they also clearly highlight some particular differences with respect to the BS process which are mainly related to the instability of the PC process. First, the idler power can significantly exceed the input signal power; and second, the idler amplification impairment induced by quick random perturbations is not a constant value but is instead proportional to the fiber length as well as to the input pump powers. More precisely, we notice that for any value of L_C the idler power (in dBm) versus fiber length is well approximated by a line with a slope that depends on L_C. Analytical considerations allow us to estimate an impairment of about $(2/3)C_{0011}(P_0P_1)^{1/2}$ between the slope in the Uncoupled Regime (when input waves are aligned to one of the birefringence axes) and the slope in the Manakov Regime. This is related to the fact that the intermodal cross phase modulation (XPM) coefficient of copolarized waves, which reads $2C_{0011}$ in the absence of random linear coupling, is reduced to $(4/3)C_{0011}$ in the Manakov limit [11], [21].[1]

Note that in [17] the authors have analyzed the PC process in presence of random perturbations characterized by $L_c = 10$ m and a residual birefringence $\Delta n = 10^{-6}$. The corresponding beat lengths are therefore of the order of $\lambda/\Delta n = 1.5$ m (for $\lambda \approx 1.5$ μm). Consequently, the authors have implicitly investigated the regime that here we call Uncoupled, where random mode coupling does not play any relevant role.

We point out that the dynamics depicted here is observed also in fibers whose length is several tens of km. Fig. 5 displays the idler amplification for the PC process in a 25-km long fiber, where several hundreds of random fluctuations occur even in the Uncoupled Regime ($L/L_c \approx 100$). The system parameters are kept unchanged, but pump and signal powers are reduced (20 dBm and -55 dBm, respectively) in order to reduce pump depletion and thus increase the length over which the idler undergoes amplification. Here the idler growth (in dBm) is not linear with the fiber length, which is due to the linear losses experienced by both the pumps and the sidebands. However, We still distinguish the 3 regimes mentioned above.

To conclude, our results indicate that the Manakov model can correctly describe the full FWM dynamics only when L_C is of the same order as the shortest beat length. On the other

[1]Note that in the weakly guiding approximation and when the Raman contribution is neglected as in our simulations the coefficient $(4/3)C_{0011}$ is found in both cases in which modes LP_{11a} and LP_{11b} are weakly coupled or strongly coupled, see Eq. (62-64) in Ref. [21].

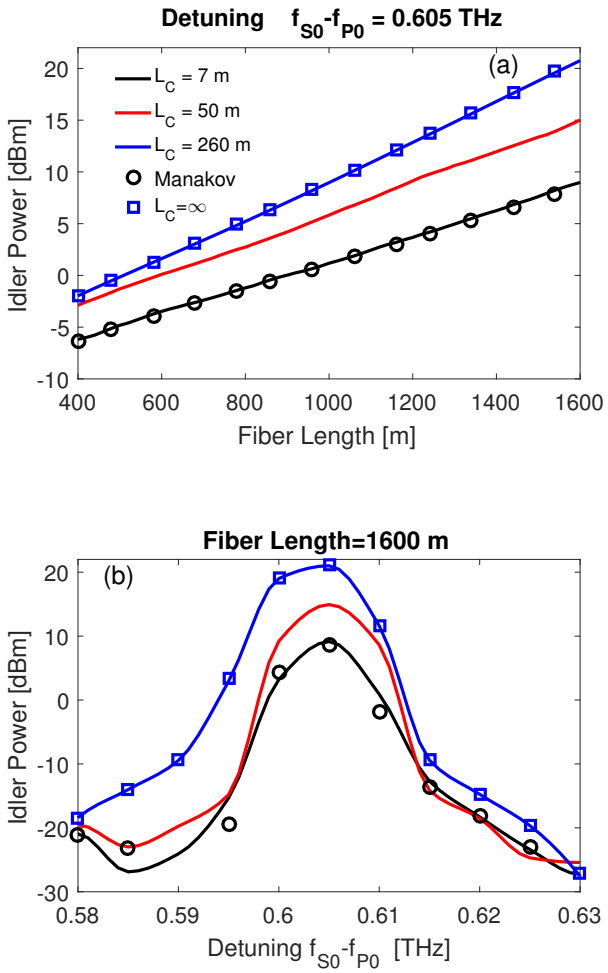

Fig. 4. PC process. (a) Idler power versus fiber length L for different values of coherence length L_C. The signal-to-pump detuning $f_{S0} - f_{P0} = 0.605$ THz maximizes the phase-matching. The pump-to-pump detuning is zero (degenerate FWM). The case $L_C = \infty$ (fixed axes of birefringence) and the solution of the multimode Manakov model are also reported. (b) Idler power versus signal-to-pump detuning for a fixed fiber length $L = 1600$ m.

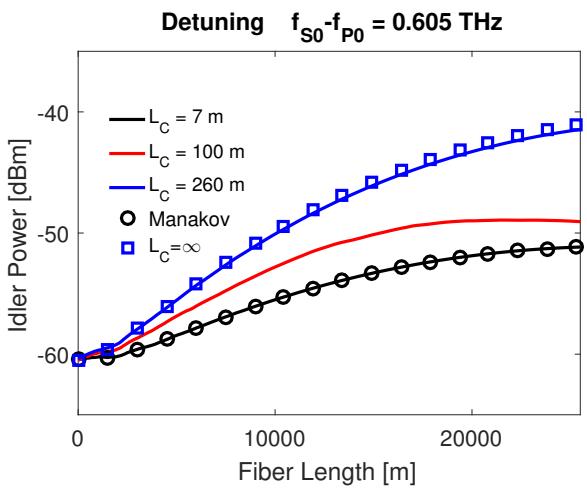

Fig. 5. Same as in Fig. 4(a) but for propagation over 25 km and with input pumps and signal powers reduced to 20 dBm and -55 dBm, respectively.

hand, even for realistic values of a few tens of meters (see e.g. $L_C = 50$ m in Figs. 3, 4) the Manakov model fails in describing the idler dynamics, which sets important boundaries on its limits of applicability.

V. Impact of Mode Dispersion

So far we have neglected mode dispersion (MD), i.e., that the random dynamics discussed in the previous sections is in reality frequency dependent, similar to the case of polarization mode dispersion in single-mode fibers.

When dealing with a group of modes that are N-fold degenerate with N>2, like the LP_{11} group, it is useful to introduce the idea of the hyper-polarization state (HPS) [21] which indicates the energy and the relative phase related to each one of the quasi-degenerate modes of the group. The HPS represents therefore a generalization of the state of polarization in single-mode fibers.

The main issue related to MD is that waves at two different frequencies undergo a different randomization: as a result, the relative HPS of the modal groups at different frequencies cannot be indefinitely preserved along the fiber.

In order to investigate MD, we resort to the definition of diffusion length $L_D = 3/(4\pi^2 D_p^2 \Delta f^2)$ that in single mode fibers indicates the length scale beyond which the relative state of polarization is not maintained as a result of polarization mode dispersion (PMD). Here Δf is the frequency detuning between the two waves and D_p the PMD coefficient that is related to the beat length through the relation $D_p = (2L_e)^{1/2}/(L_B f)$, where f is the carrier frequency of one of the two waves and L_e the polarization correlation length [33]. The latter is related to L_C and L_B according to a relation that varies depending on the regime under analysis [26]. It should be noted that the concept of PMD and diffusion length rigorously applies only to groups of linearly polarized modes that are 2-fold degenerate, whereas in 4-fold degenerate groups MD should be evaluated in terms of the intensity pulse response duration [31], [32]. However, in the multimode system considered here it proves useful to compute a diffusion length for each couple of quasi-degenerate modes in a group. Indeed the smallest, $\min\{L_D\}$, and largest, $\max\{L_D\}$, diffusion lengths allow us to distinguish two regimes: a low-MD regime, when the fiber length $L \ll \min\{L_D\}$, where the relative HPS of group of modes is preserved along the fiber; and a high-MD regime, when $L \gg \max\{L_D\}$, where the relative HPS varies randomly along the fiber.

An exhaustive analysis of the MD impact is complex and out of the scope of the current paper, therefore in the following we limit our study to the Manakov Regime, which is important for km-long fibers, and we focus on the degenerate PC process introduced in Section IV. According to the system parameters, when $L_C = 7$ m (Manakov Regime), the minimum diffusion length is several tens of km, therefore results displayed in Figs. 3, 4 concern the low-MD regime. In order to move towards the high-MD regime of the PC process we keep the system parameters unchanged except for the group velocity mismatch $v_{0p} - v_{1ap}$ that is set to 1640 ps/km (such a large mismatch may be found in step-index fibers). Consequently,

the phase matching detuning $\Delta f = f_{S0} - f_{PO}$ increases to 10 THz and the corresponding largest diffusion length $\max\{L_D\}$ decreases to 725 m. In Fig. 6(a) the idler power versus fiber length is displayed for different realizations of the orientation angle $\alpha(z)$ that are *all* characterized by the same correlation length $L_C = 7$ m. Differently from the low-MD regime, where the idler growth is almost independent of the particular realization, the high-MD regime is characterized by severe variations of the idler amplification from one realization to another. **Since Raman contribution is ignored in our simulations, these variations are unambiguously related to the interplay between FWM and MD**. Note that a similar dynamics has been previously observed in single-mode fibers [34]. Furthermore, from Fig. 6(b) we notice that the idler growth, averaged over a consistent number of different realizations, is generally reduced by several dB due to MD. The impairment is proportional to the fiber length and can be as large as several tens of dB at the output of a km-long fiber. These results clearly indicate that, while IM-FWM can potentially be phase matched far away from the zero dispersion wavelength, in practice broadband operation in km-long fibers is strongly limited by MD.

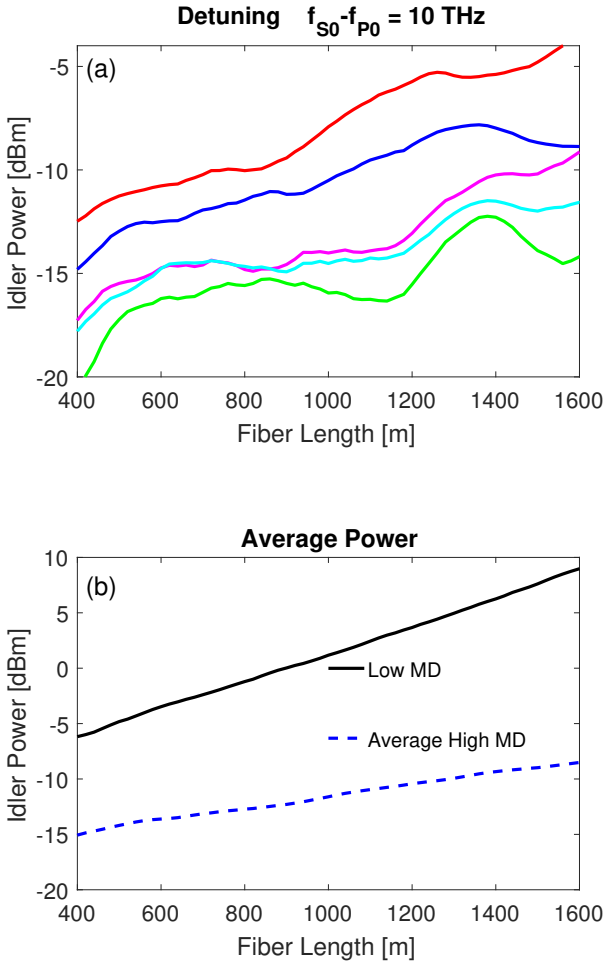

Fig. 6. (a) Idler power versus fiber length L of the PC process in the high-MD regime. Five different curves are displayed, each one corresponding to a different random realization of the function $\alpha(z)$ for the same correlation length $L_C = 7$ m. System parameters are the same as for results displayed in Fig. 4(a), except for the group-velocity mismatch $v_{0p} - v_{1ap}$ that have been modified to shift the phase-matching detuning $f_{S0} - f_{P0}$ to 10 THz. (b) Comparison between the idler power in the low-MD regime (phase matching detuning $f_{S0} - f_{P0} = 0.605$ THz, see also Fig. 4) and the power averaged over 60 realizations in the high-MD regime (phase matching detuning $f_{S0} - f_{P0} = 10$ THz).

VI. Impact of the Variation of Dispersive Parameters

The study of random perturbations portrayed in previous sections was based on the assumption that the dispersion parameters were constant along the fiber length ($\tilde{\boldsymbol{\beta}} = \tilde{\boldsymbol{\beta}}_{\mathbf{1}} = \tilde{\boldsymbol{\beta}}_{\mathbf{2}} = 0$ in Eq. (2)). More realistically however, random local perturbations affect these dispersion parameters [9], [35], [36] and we will study the impact of this z-dependence in the following.

Towards this, we distinguish the *intragroup dispersive parameters*, which are the beat lengths ($L_{B(0p-0o)}$, $L_{B(1ap-1ao)}$, $L_{B(1ap-1bp)}$, $L_{B(1ap-1bo)}$) and the relative inverse group velocities ($\beta_{1,0p}-\beta_{1,0o}$, $\beta_{1,ap}-\beta_{1,ao}$, $\beta_{1,ap}-\beta_{1,bp}$, $\beta_{1,ap}-\beta_{1,bo}$) among quasi-degenerate modes of the same group, and the *intergroup dispersive parameters* $\beta_{1,0p}$, $\beta_{1,ap}$, $\beta_{2,0}$ and $\beta_{2,1}$, which describe the different dispersive properties of different modal groups.

As pointed out in Section IV, the IM-FWM dynamics at phase-matching depends on the intragroup parameters, more precisely the beat lengths, so that three distinct regimes can be distinguished which we called the Uncoupled, Manakov, and Intermediate Regimes. On the other hand, the phase matching condition for the BS and PC processes between LP_{01} and LP_{11} modes depends on the intergroup parameters but is practically unaffected by intragroup parameters. Therefore, we proceed by studying separately the effect of the z-dependence of the intergroup and intragroup parameters.

Initially, Eq. (2) is solved by keeping the intergroup parameters fixed while varying the intragroup parameters $\tilde{\boldsymbol{\beta}}$ and $\tilde{\boldsymbol{\beta}}_{\mathbf{1}}$ with z. In order to implement the z-dependence, each intragroup parameter is defined as a random function $p(z)$ with spatial average $\bar{p}$, standard deviation $\sigma(p)$ and correlation length L_C. Our numerical simulations show that the IM-FWM dynamics is not sensitive to local variations of the intragroup parameters, but only to their average value. We verified numerically that this is true even for standard deviations which are as large as the average value. It is worth noting that this outcome is in line with previous studies in single-mode fibers [26]. Therefore, we still recognize the three regimes found in Section IV, provided that the values of the beat lengths are replaced by their spatial averages, so that the thresholds for the Uncoupled and Manakov regimes become $L_C > 5\max\{\bar{L}_B\}$ and $L_C < \min\{\bar{L}_B\}$, respectively.

Contrary to the case of intragroup parameters, even small variations of the intergroup parameters can strongly impact the phase-matching condition and then severely affect the IM-FWM dynamics. This issue has already been addressed in single-mode fibers, where small fluctuations of the chromatic dispersion along the fiber can lead to a remarkable reduction of the idler amplification bandwidth [9], [35]. In the multi-

mode dynamics this issue is even more critical, as the idler amplification band depends on all four intergroup parameters, that is, not only on the chromatic dispersion coefficients but also on the group velocities of groups LP_{01} and LP_{11} [4].

As a practical example, we consider here a 1-km long MM silica step-index fiber whose core radius $R(z)$ varies randomly in z, thereby inducing fluctuations of the intergroup parameters. Note that radius fluctuation is a typical perturbation occurring on a length-scale L_C of a few meters during the drawing stage of the fiber, where the standard deviation of the radius can be as large as 1% [9]. Here we assume the core radius $R(z)$ to have average $\bar{R} = 40$ μm and correlation length $L_C = 5$ m. We simulate two distinct instances where its standard deviation is either 0.5% ($\sigma(R) = 2$ μm) or 1% ($\sigma(R) = 4$ μm), respectively. The core-cladding index difference is fixed at 0.0025, independently of the wavelength. Several groups of modes can propagate in this fiber, but we assume only modes $0p$ and $1ap$ are excited and propagate. Note that in order to isolate the impact of the variation of intergroup parameters here we do not introduce random linear coupling among quasi-degenerate modes (i.e. we set $\partial_z \alpha = 0$ in Eq. (2)). We calculate the intergroup parameters and nonlinear coefficients at each position z of the fiber, and solve Eq. (2) accordingly. In order to compute the intergroup parameters at position z, we first derive the propagation constants $\beta_{0p}(z)$ and $\beta_{1ap}(z)$ of modes $0p$ and $1ap$ by solving the modal characteristic equation for a circular-core fiber of radius $R(z)$; we then directly infer the intergroup parameters $\beta_{1,0p}(z) = \partial\beta_{0p}/\partial\omega$, $\beta_{1,1ap}(z) = \partial\beta_{1ap}/\partial\omega$, $\beta_{2,0} = \partial^2\beta_{0p}/\partial\omega^2$ and $\beta_{2,1} = \partial^2\beta_{1ap}/\partial\omega^2$ by also taking into account the material dispersion of silica. Similarly, in order to compute the nonlinear coefficients we first calculate the transverse mode profiles as a function of $R(z)$ and then the nonlinear overlap integrals. In this way, our numerical simulations also account for the z-dependence of the nonlinear coefficients. We do this for completeness, however we anticipate that these fluctuations of the nonlinearity have very little effect on the IM-FWM dynamics, so that in practice their average value could safely be used in simulations.

When solving Eq. (2) for the BS process, we fix the pump-to-pump detuning to $f_{P0} - f_{P1} = 1.65$ THz, which corresponds to the phase matching condition for a fiber with constant radius $R = \bar{R} = 40$ μm. In Fig. 7(a) the output idler power is plotted versus the signal-to-pump detuning in both the cases of fixed and varying radius. We note that the idler amplification bandwidth is only slightly impaired by fluctuations of the intermodal parameters. When repeating the same analysis with a bimodal fiber of average radius $\bar{R} = 10$ μm (phase-matching at $f_{P0} - f_{P1} = 5.095$ THz) and standard deviation 0.5% or 1% (that is $\sigma(R) = 0.05$ μm or $\sigma(R) = 0.1$ μm, see Fig. 7(b)), we find instead that the amplification bandwidth is severely reduced. This is explained by the fact that the smaller the radius, the more the modes spread out in the outer core, such that their dispersion parameters become strongly sensitive to variations of the core size. Consequently, the phase matching condition cannot be preserved along the fiber length, which causes the drastic reduction of bandwidth. Note that almost the same results are found when introducing linear coupling among quasi-degenerate modes, except for an amplification impairment of about -3.5 dB, as pointed out in Section IV.

It is worth noting that in Ref. [4] the authors have studied the BS process in a 1-km long bimodal fiber and found that the experimental bandwidth at -3 dB was about 4 times narrower than the bandwidth estimated in numerical simulations when considering the propagation in a totally uniform fiber. They then conjectured that fluctuations of the dispersive parameters may be the principal source of the observed discrepancy. The plots in Fig. 7(b), related to the bimodal fiber of average $\bar{R} = 10$ μm, give support to this interpretation.

More general, the results displayed in Fig. 7 demonstrate that the analysis of the device robustness against fluctuations of the relative intergroup dispersive parameters is an essential step when designing multimode parametric devices in km-long fibers. It is worth noting from Fig. 7(b) that these fluctuations may completely suppress the idler growth even when the frequency detuning among waves is low (that is, in a low-MD regime). Therefore they may constitute the dominant factor of bandwidth impairment in parametric amplifiers. On the other hand, the same effect may be an interesting tool to exploit in order to reduce FWM impairments in SDM transmissions.

VII. Conclusion

In this paper we studied the IM-FWM dynamics taking place between different groups of modes in a km-long MMF. This work has been motivated by the possibility to achieve consistent IM-FWM effects at low input powers in these fibers. This may have both positive implications, if we target the development of efficient mode converters and amplifiers, as well as a negative side, if we think of SDM long-haul transmission. For this reason, we have focused our attention on the peculiar features that distinguish these fibers from short ones as well as on the main sources of IM-FWM impairments. We have investigated separately the impact of random fluctuations of the birefringence axes and of random fluctuations of the dispersion parameters of different groups of modes.

The former leads to a random linear coupling among quasi-degenerate modes. We identified three distinct regimes which depend on the relative magnitude between the correlation length L_C of random longitudinal fiber fluctuations and the beat lengths of the interacting quasi-degenerate modes. We then demonstrated that the Manakov model can reproduce the FWM dynamics only when L_C is of the same order of or shorter than the smallest beat length. On the contrary, when L_C is much longer than all beat lengths, the fiber acts as a birefringent fiber with fixed axes of birefringence where the IM-FWM dynamics strictly depends on the relative polarization of the input waves with respect to the axes of birefringence (Uncoupled Regime). The maximum amplification impairment between the Uncoupled and the Manakov regime varies depending on the kind of FWM process being considered: for BS processes it is about -3.5 dB almost independently of the fiber length and input pump powers, whereas for PC processes it is directly proportional to both

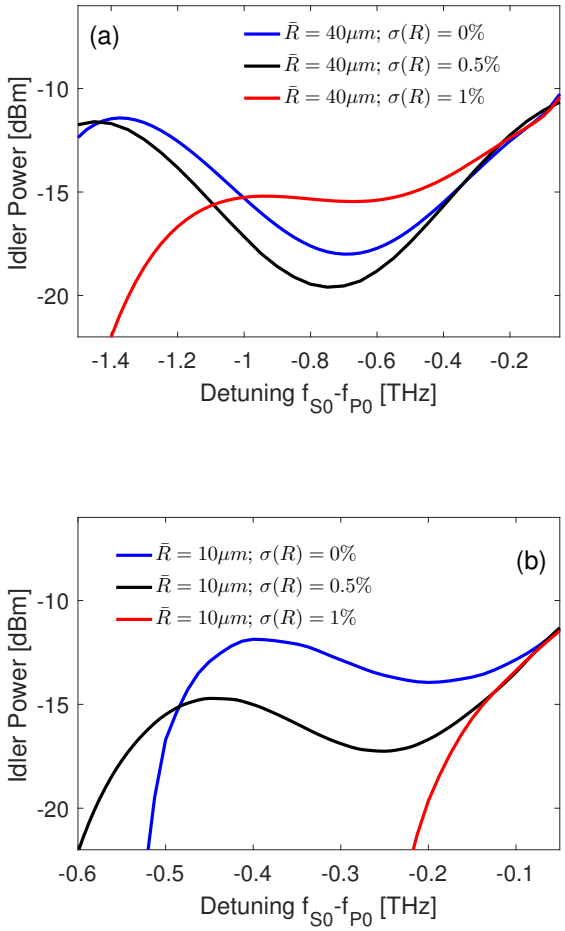

Fig. 7. Idler power versus signal-to-pump detuning for the BS process at the fiber output. The cases of fixed radius and z-varying radius ($\sigma(R)$=0.5% and $\sigma(R)$=1%) are displayed. In (a) the average radius $\bar{R} = 40$ μm; in (b) $\bar{R} = 10$ μm.

the fiber length and the pump powers. Mode dispersion is a further source of impairment: in the high-MD regime not only is the amplification substantially reduced, but it also depends on the particular longitudinal profile of the fiber perturbations. Therefore, two different profiles $\alpha(z)$ with the same correlation length may lead to strongly different FWM amplification. Finally, we found that random fluctuations of the dispersion parameters can result in a severe reduction of the FWM bandwidth and thus constitutes one of the major issues when addressing the design of efficient multimode devices for parametric amplification/conversion.

Overall, these results could find useful application in the design of mode converters and amplifiers, where one wants to control (and typically maximize) the degree of amplification. From this point of view it is essential to minimize the longitudinal fluctuations of the dispersion parameters, and to limit the detuning in a bandwidth where mode dispersion is negligible. Once this is done, the idler growth is proportional to the ratio between L_C and the beat lengths (Fig. 3,4). The Uncoupled Regime promises the largest idler growth; however, it is strongly dependent on the input polarization of pumps and signal with respect to the birefringence axes. On the other hand, in the Manakov Regime the idler growth depends only on the relative polarization among pumps and signal. These outcomes may also serve as guidelines for the study of SDM transmission where one wants to minimize the generation of parasitic idler components due to IM-FWM. In this case, a large degree of randomicity (i.e. small L_C) allows reducing the idler generation. Moreover, intentional longitudinal fluctuations of the fiber radius introduced at the drawing stage may provide consistent fluctuations of the dispersion parameters, which in turn may result in a reduction of the aforementioned parasitic effects. Finally, the finding of different FWM regimes that are not captured by the Manakov model raises important questions on its limits of validity and paves the way towards novel and robust transmission formats in multimode systems, similar to what was recently demonstrated in single-mode fibers [22].

Appendix I: Linear Coupling Matrix

Here we provide the derivation of the matrix $\mathbf{P}$ which accounts for the linear random coupling among quasi-degenerate modes of the same group. In the following we discuss the matrix coefficients related to the group LP_{11}, but a similar procedure may be used to compute the coefficients related to any group of quasi-degenerate modes. We refer to Fig. 1 for the notation. The transverse electric field of the LP_{11} modes in the segment s_n can be written as follows: $\mathbf{e_{ap}} = f(r)\sin(\alpha)\hat{\mathbf{y}}$; $\mathbf{e_{bp}} = f(r)\cos(\alpha)\hat{\mathbf{y}}$; $\mathbf{e_{a0}} = f(r)\sin(\alpha)\hat{\mathbf{x}}$;$\mathbf{e_{b0}} = f(r)\cos(\alpha)\hat{\mathbf{x}}$, where r and α are the cylindrical coordinates in the transverse plane of the fiber; $f(r)$ is the radial profile of the field; $\hat{\mathbf{x}}$ and $\hat{\mathbf{y}}$ are unit vectors aligned orthogonal and parallel to the fast birefringence axis, respectively.

Similarly, in the segment s_{n+1} the modes can be written as follows: $\mathbf{e'_{ap}} = f(r)\sin(\alpha - \Delta\alpha)\hat{\mathbf{y}}'$; $\mathbf{e'_{bp}} = f(r)\cos(\alpha - \Delta\alpha)\hat{\mathbf{y}}'$; $\mathbf{e'_{a0}} = f(r)\sin(\alpha - \Delta\alpha)\hat{\mathbf{x}}'$;$\mathbf{e'_{b0}} = f(r)\cos(\alpha - \Delta\alpha)\hat{\mathbf{x}}'$, where $\hat{\mathbf{x}}' = \cos(\Delta\alpha)\hat{\mathbf{x}} + \sin(\Delta\alpha)\hat{\mathbf{y}}$ and $\hat{\mathbf{y}}' = -\sin(\Delta\alpha)\hat{\mathbf{x}} + \cos(\Delta\alpha)\hat{\mathbf{y}}$ are the unit vectors aligned to the birefringence axes of segment s_{n+1} which are rotated by $\Delta\alpha = \alpha_{n+1} - \alpha_n$ with respect to the birefringence axes of segment s_n. As pointed out in Section III, we assume that the radial profile $f(r)$ is almost unaffected by weak perturbations, so that it can be considered constant along the fiber length.

By exploiting the relations $\sin(\alpha - \Delta\alpha) = \sin(\alpha)\cos(\Delta\alpha) - \cos(\alpha)\sin(\Delta\alpha)$ and $\cos(\alpha - \Delta\alpha) = \cos(\alpha)\cos(\Delta\alpha) + \sin(\alpha)\sin(\Delta\alpha)$, it is straightforward to re-write the modes $\mathbf{e'_{ap}}$, $\mathbf{e'_{bp}}$, $\mathbf{e'_{a0}}$ and $\mathbf{e'_{b0}}$ in segment s_{n+1} as linear combinations of the modes $\mathbf{e_{ap}}$, $\mathbf{e_{bp}}$, $\mathbf{e_{a0}}$ and $\mathbf{e_{b0}}$ in segment s_n. The coefficients of the decomposition are those reported in matrix $\mathbf{P}$ of Eq. (1).

An alternative method to derive the coefficients of matrix $\mathbf{P}$ is based on the orthogonality relation between the modes of each group. Under the assumption that coupling between different groups is negligible, the modes of group LP_{11} in one segment form a complete and orthogonal basis for the modes of the same group in another segment. Therefore, the

modes of group LP_{11} in segment s_{n+1} can be written as a linear combination of the modes of group LP_{11} in segment s_n, e.g. $\mathbf{e'_{ap}} = \sum c_{ij}\mathbf{e_{ij}}$ (i={a,b},j={p,o}). According to the orthogonality relation [37], $\int_S \mathbf{e_{ij}} \times \mathbf{h_{kl}}^* \partial\mathcal{S} = 0$ whenever $i \neq k$ or $j \neq l$, where integration is computed over the transverse plane $\mathcal{S}$. The transverse magnetic fields $\mathbf{h}$ read similarly to their electrical counterparts but are rotated of $\pi/2$ over the transverse plane, e.g. $\mathbf{h_{ap}} = g(r)\cos(\alpha)\hat{\mathbf{x}}$, $g(r)$ being the radial profile of the LP_{11} magnetic field. We multiply both sides of the linear combination above by $\times\mathbf{h^*_{1ij}}$, integrate over the transverse plane and exploit the orthogonal condition. Finally, the coefficients of the linear combination read as $c_{ij} = (\int_S \mathbf{e'_{ap}} \times \mathbf{h^*_{ij}}\partial\mathcal{S})/(\int_S \mathbf{e_{ij}} \times \mathbf{h^*_{ij}}\partial\mathcal{S})$, and are those reported in matrix $\mathbf{P}$ of $Eq.(1)$.

The matrix $\mathbf{U}$ is related to the matrix $\mathbf{P}$ through the limit $\partial\mathbf{A}/\partial z = \lim_{\Delta z\to 0}(\mathbf{A^{(in)}_{n+1}} - \mathbf{A^{(in)}_n})/\Delta z$ that gives rise to Eq. (2). This limit is decomposed in a sum of different terms, one of which reads $\lim_{\Delta z\to 0}(\mathbf{P} - \mathbf{I})/\Delta z$, where $\mathbf{I}$ is the 6x6 identity matrix. Taking into account that: $\lim_{\Delta z\to 0}\sin(\Delta\alpha)/\Delta z = \Delta\alpha/\Delta z = \partial_z\alpha$, and similarly, $\lim_{\Delta z\to 0}\sin^2(\Delta\alpha)/\Delta z = 0$ and $\lim_{\Delta z\to 0}\sin(\Delta\alpha)\cos(\Delta\alpha)/\Delta z = 1$, we finally find that $\lim_{\Delta z\to 0}(\mathbf{P} - \mathbf{I})/\Delta z = \partial_z\alpha\mathbf{U}$, where the matrix $\mathbf{U}$ takes the following form:

$$\mathbf{U} = \begin{bmatrix} 0 & -1 & 0 & 0 & 0 & 0 \\ 1 & 0 & 0 & 0 & 0 & 0 \\ 0 & 0 & 0 & -1 & -1 & 0 \\ 0 & 0 & 1 & 0 & 0 & -1 \\ 0 & 0 & 1 & 0 & 0 & -1 \\ 0 & 0 & 0 & 1 & 1 & 0 \end{bmatrix} \tag{3}$$

ACKNOWLEDGMENTS

The data for this work is accessible through the University of Southampton Institutional Research Repository (DOI:xxxxxx)

REFERENCES

[1] D. J. Richardson, J. M. Fini and L. E. Nelson, *Space-division multiplexing in optical fibres*, Nature Photon. 7, 354-362 (2013).

[2] S. Wabnitz and B. J. Eggleton, *All-optical signal processing*, Springer (2015).

[3] A. D. Ellis, N. Mac Suibhne, F. C. Garcia Gunning, and S. Sygletos, *Expressions for the nonlinear transmission performance of multi-mode optical fiber*, Opt. Exp. 21, 22834-22846 (2013).

[4] S. M. M. Friis, I. Begleris, Y. Jung, K. Rottwitt, P. Petropoulos, D. J. Richardson, P. Horak and F. Parmigiani, *Inter-modal four-wave mixing study in a two-mode fiber*, Opt. Exp. 24, 30338-30349 (2016).

[5] M. Wuilpart, P. Mégret, M. Blondel, A. J. Rogers and Y. Defosse, *Measurement of the spatial distribution of birefringence in optical fibers*, IEEE Photon. Technol. Lett. 13, 836-838 (2001).

[6] A. Galtarossa and L. Palmieri, *Spatially resolved PMD measurements*, J. Lightw. Technol. 22, 1103-1115 (2004).

[7] R.-J. Essiambre, M. A. Mestre, R. Ryf, A. H. Gnauck, R. W. Tkach, A. R. Chraplyvy, Y. Sun, X. Jiang, and R. Lingle, *Experimental investigation of inter-modal four-wave mixing in few-mode fibers*, IEEE Photon. Technol. Lett. 25, 539-542 (2013).

[8] C. J. McKinstrie, H. Kogelnik, R. M. Jopson, S. Radic and A. V. Kanaev, *Four-wave mixing in fibers with random birefringence*, Opt. Exp. 12, 2033-2055 (2004).

[9] M. Karlsson, *Four-wave mixing in fibers with randomly varying zero-dispersion wavelength*, J. Opt. Soc. Am. B 15, 2269-2275 (1998).

[10] M. Guasoni, V. V. Kozlov and S. Wabnitz, *Theory of polarization attraction in parametric amplifiers based on telecommunication fibers*, J. Opt. Soc. Am. B 29, 2710-2720 (2012).

[11] Y. Xiao, R.-J. Essiambre, M. Desgroseilliers, A. M. Tulino, R. Ryf, S. Mumtaz and G. P. Agrawal, *Theory of intermodal four-wave mixing with random linear mode coupling in few-mode fibers*, Opt. Exp. 22, 32039-32059 (2014).

[12] F. Ferreira, N. Mac Suibhne, C. Snchez, S. Sygletos, and A. D. Ellis, *Advantages of Strong Mode Coupling for Suppression of Nonlinear Distortion in Few-Mode Fibers*, in Optical Fiber Communication Conference, OSA Technical Digest (Optical Society of America, 2016), paper Tu2E.3.

[13] G. Rademacher, S. Warm, and K. Petermann, *Analytical description of cross modal nonlinear interaction in mode multiplexed multimode fibers*, IEEE Photon. Technol. Lett. 24, 1929-1932 (2012).

[14] A. Mecozzi, C. Antonelli, and M. Shtaif, *Nonlinear propagation in multi-mode fibers in the strong coupling regime*, Opt. Exp. 20, 11673-11678 (2012).

[15] E. Nazemosadat, H. Pourbeyram, and A. Mafi, *Phase matching for spontaneous frequency conversion via four-wave mixing in graded-index multimode optical fibers*, J. Opt. Soc. Am. B 33, 144-150 (2016).

[16] W. Pan, Q. Jin, X. Li, and S. Gao, *All-optical wavelength conversion for mode-division multiplexing signals using four-wave mixing in a dual-mode fiber*, J. Opt. Soc. Am. B 32, 2417-2424 (2015).

[17] A. Trichili, M. Zghal, L. Palmieri, and M. Santagiustina, *Phase-sensitive mode conversion and equalization in a few mode fiber through parametric interactions*, IEEE Phot. Journal 9, 7800710 (2017).

[18] M. Esmaeelpour et al., *Power Fluctuations of Intermodal Four-Wave Mixing in Few-Mode Fibers*, in J. Lightwave Technol. 35, 2429-2435 (2017).

[19] S. Mumtaz, R.-J. Essiambre, G. P. Agrawal, *Nonlinear propagation in multimode and multicore Fibers: generalization of the Manakov equations*, J. Lightw. Technol. 31, 398-406 (2013).

[20] A. Mecozzi, C. Antonelli and M. Shtaif, *Coupled Manakov equations in multimode fibers with strongly coupled groups of modes*, Opt. Exp. 20, 23436-23441 (2012).

[21] C. Antonelli, A. Mecozzi and M. Shtaif, *Modeling of Nonlinear Propagation in Space-Division Multiplexed Fiber-Optic Transmission*, J. Lightw. Technol. 34, 3654 (2016).

[22] M. Gilles, P. Y. Bony, J. Garnier, A. Picozzi, M. Guasoni and J. Fatome, *Polarization domain walls in optical fibres as topological bits for data transmission*, Nat. Photon. 11, 102-107 (2017).

[23] L. Palmieri and A. Galtarossa, *Coupling effects among degenerate modes in multimode optical fibers*, IEEE Photon. J. 6, 0600408 (2004).

[24] L. Palmieri, *Coupling mechanism in multimode fibers*, Proc. SPIE 9009, 90090G (2014).

[25] C. Antonelli, A. Mecozzi, M. Shtaif, and P. J. Winzer, *Random coupling between groups of degenerate fiber modes in mode multiplexed transmission*, Opt. Exp. 21, 9484-9490, (2013).

[26] P. K. A. Wai and C. R. Menyuk, *Polarization mode dispersion, decorrelation, and diffusion in optical fibers with randomly varying birefringence*, J. Lightw. Technol. 14, 148-157 (1997).

[27] F. Poletti and P. Horak, *Description of ultrashort pulse propagation in multimode optical fibers*, J. Opt. Soc. Am. B 25, 1645-1654 (2008).

[28] C. J. McKinstrie, S. Radic, and A. R. Chraplyvy, *Parametric amplifiers driven by two pump waves*, IEEE J. Sel. Top. Quantum Electron. 8, 538-547 (2002).

[29] F. Parmigiani, Y. Jung, S.M.M. Friis, Q. Kang, I. Begleris, P. Horak, K. Rottwitt, P. Petropoulos, and D.J. Richardson,*Study of Inter-Modal Four Wave Mixing in Two Few-Mode Fibres with Different Phase Matching Properties*, ECOC 2016, European Conference and Exhibition on Optical Communications (2016)

[30] L. Su, K.S. Chiang, and C. Lu *Microbend-induced mode coupling in a graded-index multimode fiber*, Appl.Opt.44,7394-7402 (2005)

[31] R. Ryf et al., *Mode-division multiplexing over 96 km of few-mode fiber using coherent 6 6 MIMO processing*, J. Lightw. Technol. 30, 521-531 (2012).

[32] A. Mecozzi, C. Antonelli, and M. Shtaif, *Intensity impulse response of SDM links*, Opt. Exp. 23, 5738-5743, (2015).

[33] G. P. Agrawal, *Nonlinear Fibre Optics, 4th Edition*, Elsevier (2007).

[34] Q. Lin and G. P. Agrawal, *Effects of polarization-mode dispersion on fiber-based parametric amplification and wavelength conversion*, Opt. Lett. 29, 1114-1116 (2004).

[35] F. Yaman, Q. Lin, S. Radic and G. P. Agrawal, *Impact of dispersion fluctuations on dual-pump fiber-optic parametric amplifiers*, IEEE Photon. Techol. Lett. 16, 1292-1294 (2004).

[36] E. Myslivets and S. Radic, *Spatially Resolved Measurements of the Chromatic Dispersion in Fibers*, J. Lightw. Technol. 33, 597-608, (2015).

[37] D. Marcuse, *Theory of Dielectric Optical Waveguides*, Academic Press (1974).